ELSEVIER

Contents lists available at ScienceDirect

Journal of Environmental Chemical Engineering

journal homepage: www.elsevier.com/locate/jece





Effects of various carbon-supported iron catalysts on tar removal efficiency and syngas yield during catalytic biomass gasification

Afsaneh Khajeh ^a, Shima Masoumi ^b, Lijun Wang ^{b,c,*}, Abolghasem Shahbazi ^{b,c}

- ^a The Joint School of Nanoscience and Nanoengineering, North Carolina Agricultural and Technical State University, Greensboro, NC, USA
- b Department of Natural Resources and Environmental Design, North Carolina Agricultural and Technical State University, Greensboro, NC, USA
- ^c Department of Chemical, Biological and Bioengineering, North Carolina Agricultural and Technical State University, Greensboro, NC, USA

ARTICLE INFO

Editor: Chao He

Keywords: Catalytic gasification Syngas Tar removal Iron catalysts Carbon support Biochar

ABSTRACT

Raw biomass, biochar, and activated carbon (AC) were used to produce carbon supported iron catalysts for catalytic biomass gasification. K_2CO_3 was used to activate the biochar and provide the K promoter of the catalysts. The results showed that the catalyst prepared by co-impregnating and calcining Fe and K on the raw biomass (B-Fe-K) could remove 80.23 % tar, which was much higher than 73.73 % for the catalyst of B-Fe without the K promoter, and 76.25 % for the catalyst by co-impregnating and calcining Fe and K on the biochar (C-Fe-K). The supports of AC and biochar themselves could also remove 63.16 % and 37.23 % tar, respectively. The use of B-Fe-K almost doubled the syngas yield to 473.79 ml/g (including 243.56 ml/g CO, 198.25 ml/g H₂, and 31.98 ml/g CO₂), compared to 241.37 ml/g syngas (including 108.98 ml/g CO, 66.41 ml/g H₂, and 65.987 ml/g CO₂) produced by the pyrolysis of biomass without a catalyst. The addition of biochar during the pyrolysis slightly increased the syngas yield to 248.96 ml/g (117.36 ml/g CO, 74.22 ml/g H₂, and 57.38 ml/g CO₂) while the use of AC could significantly increase the syngas yield to 347.60 ml/g (179.39 ml/g CO, 124.22 ml/g H₂, and 43.99 ml/g CO₂). It was found that the porosity, dispersion of active sites and the oxidation state of iron oxide are substantial factors determining the performance of catalysts in tar removal efficiency. The addition of potassium and enhancing the porosity of the catalysts enhanced the reducibility of iron resulted in increasing the tar removal efficiency and gas yield.

1. Introduction

There are increasing studies to develop sustainable energy sources such as biomass as an alternative to fossil energy sources [1,2]. Biomass is the only carbon containing renewable energy source which is also inexpensive and highly available. Gasification has been considered as a promising thermochemical technology to convert biomass to a high value gaseous product of syngas (mainly CO, H_2 , CO_2 , and CH_4) [3,4]. However, biomass gasification produces an undesirable by-product of tar, which has many side-effects on the downstream uses of syngas such as pipeline blockage, corrosion, catalyst deactivation, and lowering gasification efficiency [5,6].

Catalysts play a vital role to enhance syngas production and tar removal during biomass gasification. Various catalysts have been studied to decompose heavy tar compounds such as aromatics into syngas. Al_2O_3 is usually used as a catalyst support due to its favorable

physicochemical properties and excellent stability, but Al₂O₃ supported catalysts experience the ease deactivation caused by coke deposition [6, 7].

Carbon-based metal catalysts have attracted much attention for catalytic tar cracking recently. Biochar, a by-product of biomass gasification, has attracted a great attention for the catalytic destruction of tar because of its low cost and high availability [8–10]. Biochar has been studied as an active catalyst for tar reforming to convert tar into gaseous products [11]. Moreover, biochar-supported oxygen carriers were found to significantly increase syngas yield while reduce tar and char yields during the gasification of wood chips. At a high temperature, the biochar can serve as a catalyst to crack tar molecules and as a solid fuel to react with CO_2 to produce CO via the Boudouard reaction, which improve the quality and energy content of the syngas [12]. It was reported that a rice husk-derived biochar catalyst could reduce tar formation and transform large polycyclic aromatic hydrocarbons (PAHs) to lighter tar molecules

E-mail address: lwang@ncat.edu (L. Wang).

^{*} Corresponding author at: Department of Natural Resources and Environmental Design, North Carolina Agricultural and Technical State University, Greensboro, NC. USA.

such as phenol and 4-methyl-phenol [13]. Although biochar is an inexpensive catalyst for catalytic cracking of tar in the syngas, its tar cracking reaction rate was much lower than traditional olivine and Ni-based catalysts. Therefore, the catalytic activity of biochar in tar cracking should be increased [14].

It is widely acknowledged that K-based catalysts are highly effective in promoting gasification reactions, as well as exhibiting catalytic effects on water-gas-shift and methanation reactions. It was reported that the K promoter in a catalyst could decrease the activation energy of biomass gasification and increase the active base sites to facilitate the reactions involved $\rm CO_2$. The activated energy during gasifying biochar pellets with $\rm CO_2$ decreased from 389 kJ/mol to 273 kJ/mol when the K content in the pellets increased from 0 to 20 wt% [15].

As a result, K salts are commonly incorporated into composite catalysts. Additionally, transition metal compounds, such as Fe, Co, Ni, and Ce, have been shown to possess good catalytic properties for gasification reactions, water-gas-shift reactions, and methanation reactions. The effects of temperature, pressure, steam-biomass ratio, and K-based composite catalysts were investigated for the pressurized steam gasification of sawdust char. The addition of composite catalysts was found to lower the reaction temperature and increase carbon conversion. The K-Ce composite catalyst demonstrated the most superior catalytic performance, primarily due to its ability to activate carbon during pressurized steam gasification of char. K-Fe and K-Co were observed to be more conducive to water-gas-shift reactions, whereas K-Ni exhibited better performance for gasification reactions [16]. Therefore, biochar loaded with relatively cheap metals such as Ni or Fe, could significantly enhance the catalytic removal of tar [17-20]. Shen et al. [21-23] studied the tar removal efficiency over a bimetallic Ni-Fe biochar supported catalyst. Their studies showed that biochar impregnated with iron as an active metal and Ni as a promoter increased the tar cracking as promotor could facilitate the reduction of iron oxide.

Biochar obtained from biomass pyrolysis or gasification had a low porosity and poor catalytic performance. Various processing factors affect the performance of biochar in its applications as a support for oxygen carriers in CLG and adsorbent [24,25]. Heating rate and pretreatment such as torrefaction and densification are the most important factors that affect the pyrolysis product distribution and biochar characteristics. It was reported that fast pyrolysis could increase the pore volume and surface area of biochar as well as the bio-oil yield due to the minimization of secondary reactions [26]. Studies showed that the activation energy for pyrolyzing torrefied biomass was higher than that for pyrolyzing raw biomass. Furthermore, the torrefaction and densification of biomass prior to pyrolysis could improve the quality of the biomass and reduce specific energy consumption during pyrolysis [27, 28]

Physical or/and chemical activation can be used to improve the physiochemical properties of biochar [29,30]. Compared with physical activation (using H2O, CO2 or both), chemical activation (using a chemical agent such as KOH, K2CO3 and H3PO4) could effectively enhance the porous characteristics of biochar and its catalytic performance at a lower temperature [31,32]. The chemical reactions between KOH or K2CO3 and a carbonaceous material such as biomass produce K₂O and gases of CO and CO₂. The release of the gases from the material form meso- and micro pores and increase the BET surface of the biochar. The KOH that is widely used as an activating agent to produce activated carbon is primarily attributed to its potent alkaline properties. It can effectively react with O-containing functional groups in the material and thus break down the material to significantly increase its porosity and the BET surface area [33]. Various activated biochars produced by chemical or physical activation demonstrate different performance in tar removal. It was reported maximum tar decomposition efficiency up to 91.75 % has been achieved using the activated carbon (AC) produced by KOH as a chemical agent at temperature of 800 °C with a catalyst-to-feedstock ratio of 2:1 [6]. The effects of CO₂ etching over iron supported sawdust as a biomass have been studied and the results

showed that CO_2 etching improved the porous characteristics and increased the content of Fe^0 . Also, the tar conversion efficiency increased up to 90.4 % [19]. Another study on the catalytic purification of syngas over biochar and physically AC showed that compared to the biochar, the AC showed higher performance due to its higher porosity and ash content [34].

It is interesting to consider the effect of minerals such as K which inherently existe inside the biomass materials and could be more concentrated in their derived biochar. These alkali and alkaline earth metals in their oxidized forms with the oxygen-containing functional groups could facilitate the decomposition of pyrolysis volatile hydrocarbons as well as enhancing water-gas shift reaction during biomass gasification [35,36]. It was reported that yields of H2, CO and CH4 were increased during gasification in the presence of alkali and alkaline earth metals due to the enhanced polymerization and aromatization reactions of tar compounds, suppression of CO₂ generation, and promotion of the water-gas shift reactions [35]. Therefore, the preparation factors including the pyrolysis temperature, heating rate and the removal or addition of metallic minerals influence the catalyst activity in tar removal efficiency [37]. In the study of tar conversion over a bimetallic Ni-Fe biochar supported catalyst, two aspects about the role of biochar catalysts in tar cracking were proposed by Shen et al. [21–23] which are: (1) acting as an adsorbent for tar and CO₂ molecules and (2) facilitating the reduction of metal oxides.

This study was the first time to synthesize and characterize iron catalysts prepared by impregnating and calcining iron on various carbon materials of raw biomass, biochar, and AC with and without a potassium promoter. Experiments were conducted to analyze the effects of the various carbon supports used during catalyst preparation on their porosity, dispersion of active sites and the oxidation state of iron oxide and their catalytic performance for tar removal efficiency and syngas yield during catalytic biomass gasification. Furthermore, the degree of dependency of tar removal efficiency on the two operating conditions (1) reaction temperature and (2) catalyst-to-feedstock ratio was compared.

2. Materials and methods

2.1. Materials

Woody sawdust was collected from a local company in North Carolina, U.S.A. and sieved by a 2 mm mesh. The sawdust was used to prepare biochar and AC as catalyst supports, and as a biomass feedstock in catalytic gasification. Certified ACS reagent- grade ≥ 98 % of iron (III) nitrate nonahydrate (Fe(NO)_3·9 H_2O) and ACS reagent ≥ 99.0 % potassium carbonate (K_2CO_3) were purchased from Sigma-Aldrich. ACS grade hydrochloric acid with assay percentage of 37.6 % was purchased from Fischer Scientific.

2.2. Preparation of biochar, AC, and carbon supported iron catalysts

Nine samples of biochar, AC, and their supported catalysts were prepared using various processing steps. Table 1 summarizes the major processing steps used for preparing these nine samples. Biochar (sample #1) was produced by pyrolyzing the biomass in a fixed bed reactor (25 cm length \times 2 cm inside diameter) at 800°C purged with nitrogen gas at 100 ml/min. AC (sample #8) was prepared by impregnating the biochar with K_2CO_3 at a mass ratio of biochar/ K_2CO_3 of 1:1.5. The mixture was calcined in the fixed bed reactor at 700°C for 3 h under a N_2 flow at 100 ml/min. After calcination, a 1 M of HCl aqueous solution was used to wash the sample three times to remove the ash and other inorganic compounds. The removal of K residue and other minerals in the raw AC was to avoid their catalytic effects when the AC was further used as a catalyst support in this study. The sample was then washed with distilled water until its pH value became neutral. The AC was then dried at 110 °C for 24 h.

Table 1
Major processing steps for preparing biochar, AC, and their supported catalysts.

Sample #	Sample symbols	Major processing steps
1	C (biochar)	Pyrolysis of biomass to biochar at 800 °C for 2 h
2	B-Fe	1. Wet impregnation of 20 wt% Fe on biomass directly
3	C-Fe	 Calcination at 700 °C under a N₂ flow for 5 h Wet impregnation of 20 wt% Fe on the biochar Calcination at 700 °C under a N₂ flow for 5 h
4	В-К	1. Wet impregnation of K on biomass at biomass/ K ₂ CO ₃ ratio of 1:1.5
		2. Calcination at 700 $^{\circ}\text{C}$ under a N_2 flow for 5 h
5	C-K	 Wet impregnation of K on biochar at biochar/
		K ₂ CO ₃ ratio of 1:1.5
		2. Calcination at 700 °C under a N ₂ flow for 3 h
6	B-Fe-K	Wet impregnation of 20 wt% Fe on biomass
		directly
		2. Calcination at 700 °C under a N ₂ flow for 5 h
		3. Wet impregnation of K on biochar from Step 2 at
		biochar/K ₂ CO ₃ ratio of 1:1.5 4. Calcination at 700 °C under a N ₂ flow for 3 h
7	C-Fe-K	1. Wet impregnation of 20 wt% Fe on the biochar
,	G-FC-K	2. Calcination at 700 °C under a N ₂ flow for 5 h
		3. Wet impregnation of K on biochar at biochar/
		K ₂ CO ₃ ratio of 1:1.5
		4. Calcination at 700 °C under a N ₂ flow for 3 h
8	AC (activated	1. Wet impregnation of K on biochar at biochar/
	carbon)	K ₂ CO ₃ ratio of 1:1.5
		2. Calcination at 700 °C under a N2 flow for 3 h
		3. Washing with HCl aqueous solution
9	AC-Fe	1. Wet impregnation of K on biochar at biochar/
		K ₂ CO ₃ ratio of 1:1.5
		2. Calcination at 700 $^{\circ}$ C under a N $_2$ flow for 3 h
		3. Washing with HCl aqueous solution to make AC
		4. Wet impregnation of 20 wt% Fe on AC
		5. Calcination at 700 °C under a N ₂ flow for 5 h

The carbon supported catalysts were prepared using raw biomass, biochar, and AC as supports impregnated with Fe and/or K. Samples #2 B-Fe and #4 B-K were prepared by directly using raw biomass as a support in a one-pot process, which combined pyrolysis, impregnation, and carbonization. During the one-pot process, the biomass was loaded with 20 % Fe (#2) or K_2CO_3 at a biomass/ K_2CO_3 ratio of 1:1.5 (#4), stirred for 3 h, followed by drying at 105 °C for 24 h. The mixture was then pyrolyzed and calcined at 700°C for 2 h under the N_2 gas. Sample #6 B-Fe-K was also prepared using raw biomass as a support through a two-step impregnation and calcination process. Samples #3 C-Fe, #5 C-K, and #7 C-Fe-K used biochar as a support impregnated and calcined with Fe and/or K. Sample #9 AC-Fe used AC as a support impregnated and calcined with Fe. All those catalysts were prepared without acid washing to evaluate the effect of inorganic availability for their catalytic performance.

2.3. Characterization of catalysts and their supports

The catalysts were characterized to find out the effects of preparation methods on catalyst properties, and to design synthesis procedures for the development of highly efficient catalysts for biomass gasification and catalyze tar decomposition.

2.3.1. Proximate and ultimate analyses

About 2.0 g of samples was weighed in a porcelain crucible and dried in an air oven at 135 \pm 2 °C to determine the moisture content and further heated in a Muffler furnace at 600 °C for 2 h to determine the ash content. The ultimate analyses of raw biomass, biochar produced at 800 °C, and AC were conducted on an elemental analyzer (Series II CHNS/O Analyzer 2400, PerkinElmer Instruments, Shelton, CT, USA) to determine their CHNSO elemental compositions.

2.3.2. Characterization of structure and morphology

The X-ray diffraction (XRD) patterns of the crystal phases of the samples were determined by an X-ray diffractometer (D8 Discover, Bruker Optics Inc., Billerica, USA) at 40.0 kV and 40.0 mA. Diffraction patterns were verified through CuK α radiation with a wavelength of 1.5406 Å over a 20 range of 5.0–80.0° with a step size of 0.04°. A scanning electron microscopy (SEM) (Zeiss Auriga FIB/FESEM) was used to investigate the morphologic structure of the samples. The samples were placed in a high-resolution coater (Leica Sputter Coater) and coated with palladium to a thickness of 80 nm before being loaded into the SEM unit.

The surface area and the changes in textural characteristics of raw biomass, biochar, and AC were measured by the nitrogen adsorption-desorption isotherms at - 196 $^{\circ}\text{C}$ in a surface area and pore volume analyzer (ASAP 2020, Micromeritics, Norcross, GA, USA). Prior to the measurement, the samples were degassed under a vacuum at 300 $^{\circ}\text{C}$ for about 4 h to withdraw adsorbed compounds. The specific surface area and pore diameter of the samples were calculated according to the Brunauer-Emmett-Teller (BET) method.

2.3.3. Thermogravimetric analyses (TGA)

The thermal degradation profiles of biomass, biochar, and AC were measured by a TGA unit (SDT Q600, TA Instrument, New Castle, DE, USA). Approximately 10.000 ± 1.000 mg of samples was loaded in an aluminum pan and placed in the TGA furnace. Experiments were performed from an ambient temperature to 800 °C at a heating rate of 10 °C/min purging with nitrogen gas at 60 ml/min.

2.3.4. Atomic composition and iron phases by XPS

The atomic composition of raw biomass was measured using a Zeiss Auriga SEM connected with an Energy-Dispersive X-ray Spectroscopy (EDX), by bombarding the sample with an electron beam to generate a spectrum of emitted X-rays corresponding to different elements in the sample that was further used to identify and quantify the elements by the EDX software. An X-ray photoelectron spectroscopy (XPS, Escalab Xi+, Thermo Scientific) was used to measure the atomic compositions of the catalysts. The samples were placed into the chamber of the XPS analyzer under a high vacuum. For each elemental analysis, the pass energy, number of scans, and dwell time were set at 20 ev, 10 and 5 ms, respectively.

2.4. Catalytic biomass gasification

Experiments on catalytic biomass gasification were carried out with a micro-tubular reactor (Multi-Shot Pyrolyzer, PY-3030, Frontier Laboratories Ltd, Fukushima, Japan), connected with a gas chromatography (GC)-mass spectrometer (MS)-thermal conductivity detector (TCD) unit (Agilent 7890 A, Agilent, Santa Clara, CA, USA). Biomass and the catalysts were mixed at 0.5:1, 1:1 and 2:1 mass ratio and were blended mechanically using a laboratory rotating mixer for 24 h. About 0.5 mg of mixture was then placed directly in a small sample cup and loaded into the reactor tube preheated to 800, 900, and 1000°C. The sample was shot into the preheated reactor tube and the reaction was proceeded at the set temperature for 30 s. In this reactor, the iron supported on biochar was used as both a gasifying agent and a catalyst for tar decomposition. The biomass was pyrolyzed and gasified using the lattice oxygen provided by the oxidized iron (i.e., iron oxides) and meanwhile the iron oxides were reduced. The volatile tar compounds were further decomposed on the surface of the reduced iron as a catalyst subsequently. The produced volatiles were directed toward the GC inlet to determine their contents. The inlet temperature of the GC was set at 300 °C to keep the volatiles in a gaseous state. The total flow and split ratio of the gas to the GC were $54\,\text{ml/min}$ and 50:1, respectively. The GC oven temperature was ramped from 60 to 200°C for 26 min to achieve proper interaction of gaseous molecules with the stationary phase of the GC for good separation. A MS detector with helium carrier gas was used

to identify ${\rm CO}_2$, ${\rm CO}$ and tar compounds of toluene, benzene, naphthalene, phenol, and styrene. A TCD with argon carrier gas was used to detect ${\rm H}_2$ because the thermal conductivities between helium and hydrogen are too close.

Gas yield, expressed in ml/g biomass, is a measure of the volume of gas produced for CO, H_2 and CO_2 per unit mass of biomass during gasification. The composition and volume of these gases were analyzed by using their established calibration curves. The tar removal efficiency was calculated as:

Tar removal efficiency =
$$\frac{V_{Tp} - V_{Tc}}{V_{Tr}} \times 100\%$$
 (1)

where, V_{Tp} is the volume of tar molecules generated in pyrolysis of biomass without a catalyst and V_{Tc} is the volume of tar compounds present in the system in presence of the catalysts. The volume determination for tar compounds was based on the calibration curves established for them using standard mixtures of these compounds with known concentrations and injected with liquid syringe directly to GC. The GC method was maintained in same condition as performance experiments.

3. Results and discussion

3.1. Elemental compositions of raw biomass, biochar, and activated carbon

Table 2 gives the results of the ultimate and proximate analyses. The carbon contents of biochar and AC were 87.01 wt% and 91.41 wt%, respectively, compared to 48.70 % for the raw biomass. The oxygen contents of biochar and AC were only 10.43 % and 5.37 %, compared to 44.1 % for the raw biomass. The ash content of biochar was slightly higher than that of raw biomass because of the centration of inorganic constituents by pyrolysis. The acid washing during the preparation of activated carbon could effectively reduce the ash content. Pyrolysis of biomass at 800 $^{\circ}$ C could effectively remove volatiles and produce fixed carbon in biochar and derived AC. The fixed carbon contents of the raw biomass, biochar, and AC were 19.8 %, 89.4 %, and 92.5 %, respectively.

Table 3 gives the compositions of the inorganic elements of the raw biomass, which were quantified by the EDX analysis. Potassium has been widely used as a promoter to improve the performance of iron-based catalysts. Additional potassium was added to the catalysts as the amount of inherent potassium in the raw biomass and its derived supports of biochar and activated carbon (AC) was low.

3.2. The structure and morphology of supports and their supported iron catalysts

Fig. 1 shows the XRD pattern of the raw biomass, biochar, AC, and their supported iron catalysts. The raw biomass showed two peaks at $2\theta=15.3^\circ$ and 22.4° which are attributed to the cellulose structure. However, these peaks were significantly destroyed in biochar, AC, and their supported catalysts due to the thermal decomposition [38]. Raw biochar (sample #1) and AC (sample #8) showed two broad ranges of diffraction peaks at 2θ of $(15–30^\circ)$ and $(40–50^\circ)$ which are attributed to the amorphous nature and the carbon structure of the samples,

Table 2Ultimate and proximate analysis of the samples.

Samples	Ultimate analysis (wt%)					Proximate	Proximate analysis (wt% dry-basis)	
	C	Н	N	S	O^a	Fixed Carbon	Volatile	Ash
Sawdust	48.70 ± 0.22	6.50 ± 0.15	0.71 ± 0.10	0.04 ± 0.002	44.10	19.81 ± 0.32	79.69 ± 0.35	0.51 ± 0.02
Biochar (#1)	87.01 ± 0.42	1.90 ± 0.10	0.61 ± 0.03	0.05 ± 0.001	10.43	89.40 ± 0.45	9.89 ± 0.12	0.71 ± 0.09
AC (#8)	91.41 ± 0.25	2.17 ± 0.13	0.23 ± 0.05	0.82 ± 0.05	5.37	92.50 ± 0.72	7.21 ± 0.10	0.29 ± 0.01

a By difference

Table 3Composition of inorganic elements in the raw biomass.

Element	Na	Mg	Al	K	Са	Fe
wt%	0.02	0.03	0.02	0.43	0.33	0.07

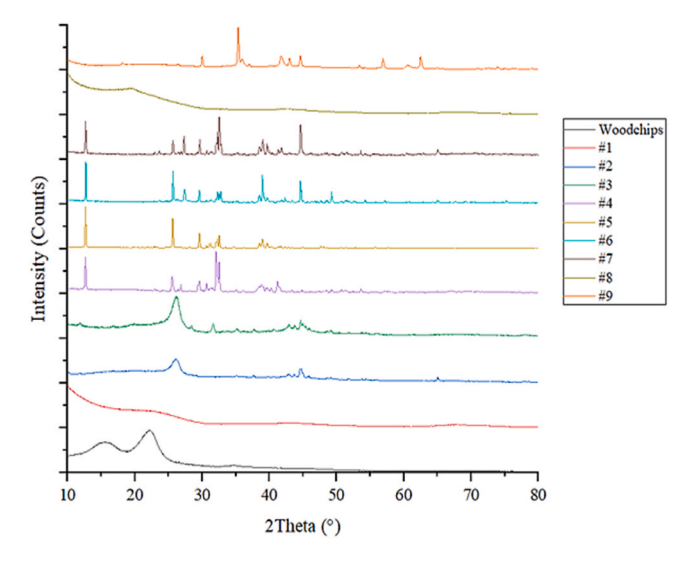
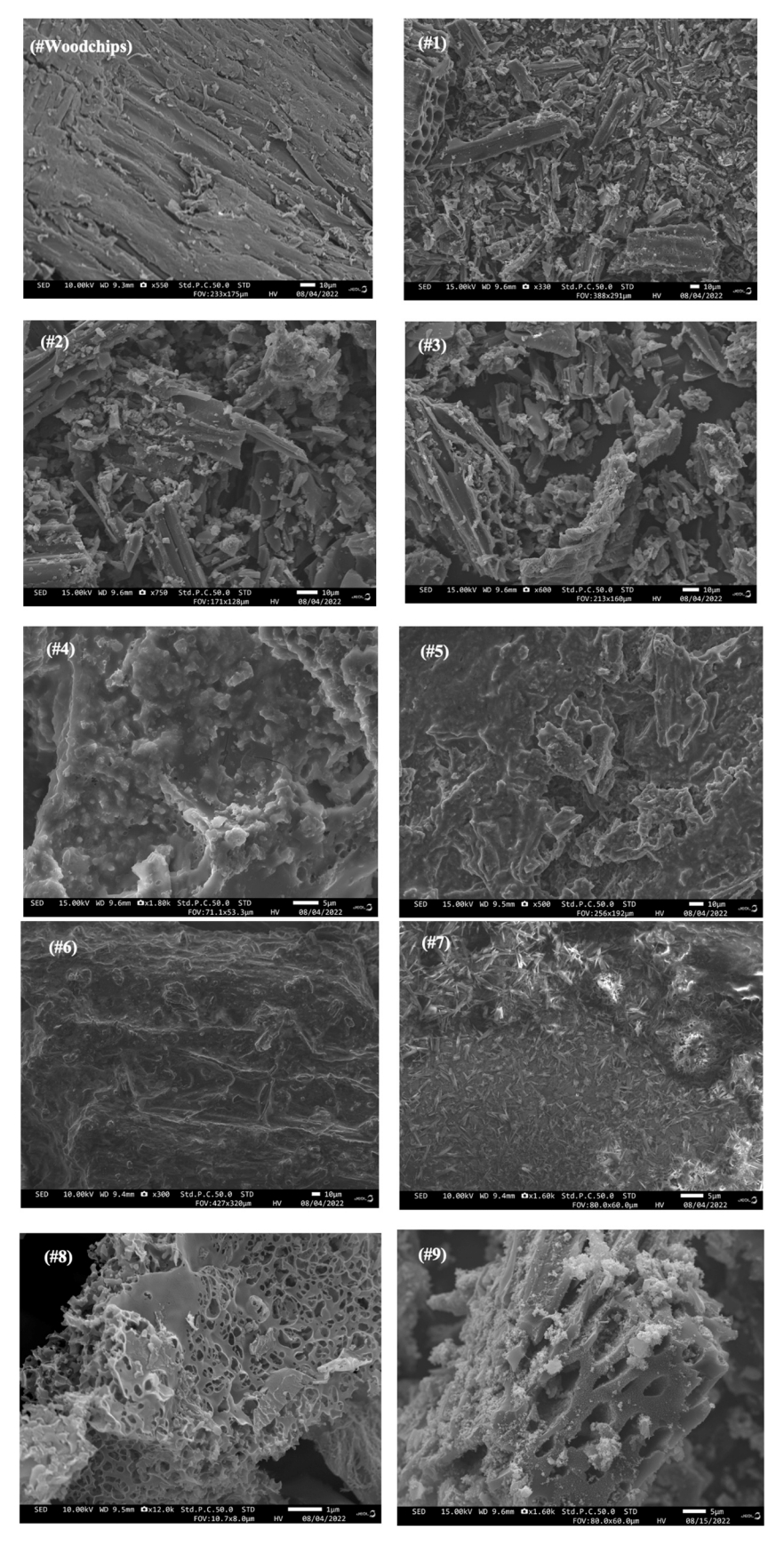


Fig. 1. XRD patterns of the raw biomass, biochar, AC, and their supported iron catalysts.

respectively [39]. The sharp peaks of other samples are attributed to the inorganic compounds as these samples were impregnated with Fe (NO₃)₅(H₂O)₉ and/or K₂CO₃. The intensity of the diffraction peaks at 20 of 36.72°, 39.72°, 42.82°, 43.64°, 57.97° and 68.76° are attributed to the reflections of iron carbide phase. The intensities of iron peaks of the Fe/AC catalysts were higher than those of Fe/biochar catalysts. This might be related to higher porous structure of AC for better dispersion of iron on the surface of the support.

Fig. 2 shows the SEM images of the samples. The surface morphology of the raw biomass is uniform with a limited porosity, compared to other samples prepared by the pyrolysis. The images of biochar sample (#1) showed irregular pore structure that was distributed over the matrix. The pores of the biochar support were filled after the impregnation with iron and/or potassium. The image of the AC (#8) showed higher porosity, indicating chemical activation process could promote the pore formation.

Table 4 gives the BET surface area, pore volume, and pore size of raw biomass, biochar, AC, and their supported catalysts. The BET surface areas of raw biomass, biochar, and AC were 4.21, 5.24, and 1201.32 $m^2/\,$ g, respectively. The BET surface area of biochar was slightly higher than that of raw biomass but the activation could significantly increase the BET surface area, which were also revealed by the SEM images given in Fig. 2. AC (#8) was produced by using K_2CO_3 as an activating agent and a HCl aqueous solution to remove the residual potassium. The chemical activation could remove a large amount of volatile compounds in the biochar, leading to an AC with a highly porous structure and high BET surface area.



 $\textbf{Fig. 2.} \ \ \textbf{SEM} \ \ \textbf{images} \ \ \textbf{of the raw biomass, biochar, AC, and their supported catalysts.}$

Table 4Porous characteristics of raw biomass, biochar, AC, and their supported catalysts.

Samples	BET Surface area (m^2/g)	Total pore volume (cm³/g)	Micropore (<2 nm) volume (cm $^3/g$)	Average pore diameter (nm)
sawdust	4.21	0.0069	0.0021	7.21
#1 (biochar)	5.24	0.0073	0.00035	5.18
#2 (B-Fe)	3.14	0.0067	0.0013	7.14
#5 (C-K)	0.191	0.0021	0.00017	12.52
#8 (AC)	1201.32	0.62	0.55	2.1
#9 (AC-Fe)	897.40	0.29	0.22	2.3

According to classification of International Union of Pure Applied Chemistry (IUPAC), pores are classified into micropore, mesopore and macropore which are in the range of (<2 nm), (2–50 nm) and (>50 nm), respectively [40]. Fig. 3 shows the adsorption-desorption isotherms of the AC. According to the isotherms, the AC can be categorized into Type-II heterogonous porous solid materials based on the IUPAC classification. There is a wide range of pore size distribution. At very low pressures, monolayer formation occurs and the micropores could be filled with the nitrogen gas during the measurement. As the pressure increased, the formation of multilayer started and finally capillary condensation took place at a higher pressure.

3.3. The thermal stability of various supports

Fig. 4 shows the thermogravimetric profiles of raw biomass, biochar, and AC, which determine the thermal stability of the materials. The biochar and AC had very low weight losses and thus very high thermal stability compared to the raw biomass.

3.4. The iron phases on the carbon-supported iron catalysts

Fig. 5 shows the XPS profiles of AC supported iron catalyst (Fe/AC). Table 5 gives the relative chemical valence and Fe 2p spectra of the biochar and AC supported iron catalysts determined by the XPS analysis. The ${\rm Fe^{2+}}$ $2p_{3/2}$ and ${\rm Fe^{2+}}$ $2p_{1/2}$ peaks were at 709.8 eV and 723.4 eV, respectively, while the peaks at 713.1 eV and 725.3 eV were the decomposition peak of ${\rm Fe^{3+}}$. The decomposition peaks at 720.0 eV and 706.6 eV correspond to ${\rm Fe_3C}$ and ${\rm Fe^0}$, respectively [17].

The catalyst that was prepared by impregnating and calcining iron on raw biomass directly (#2) had more Fe^{2+} (54.84%) than the catalyst prepared by impregnating iron on the biochar (#3) (37.08%). During calcination of iron on the supports, the raw biomass might produce more reducing agents such as CO than the biochar. The catalysts of #6 and #7 were prepared by the impregnation and calcination of iron with K_2CO_3

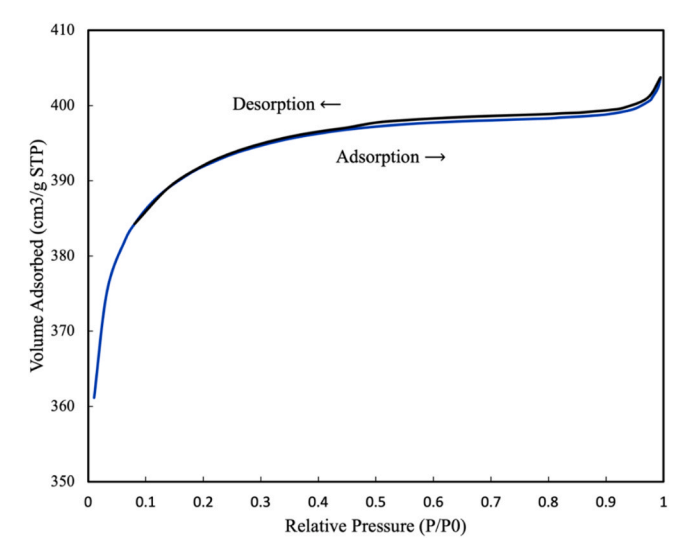


Fig. 3. Typical isotherm of chemically prepared AC (sample #8).

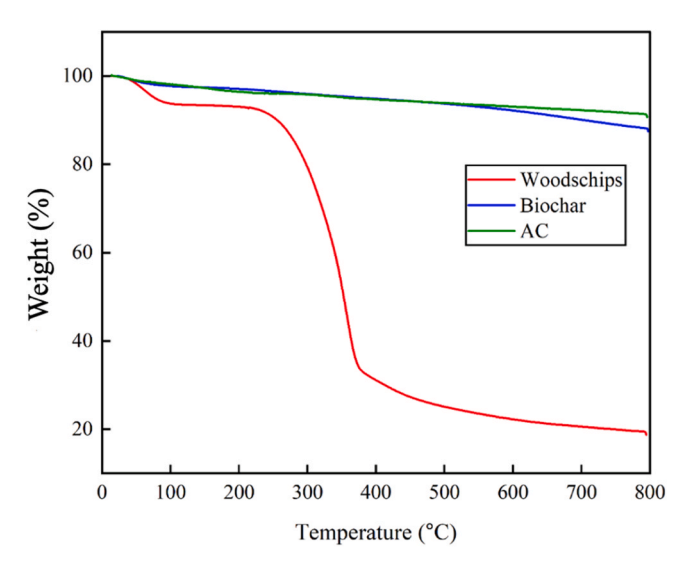
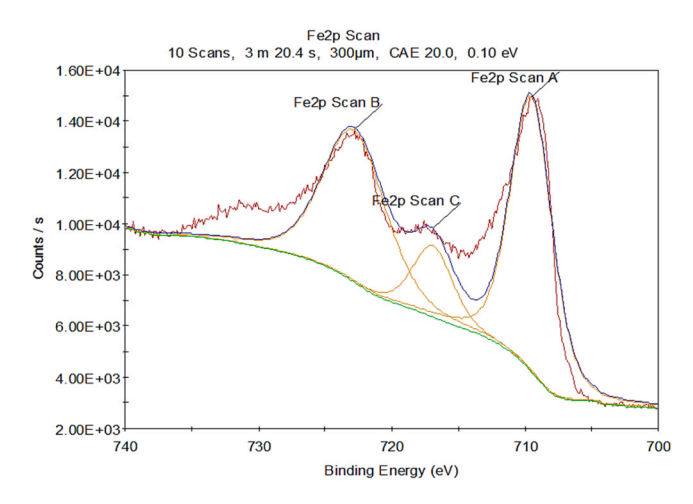


Fig. 4. Thermogravimetric analysis of the various catalyst supports.



 $\textbf{Fig. 5.} \ \ \textbf{XPS} \ \ \textbf{profiles} \ \ \textbf{the} \ \ \textbf{iron supported on AC catalyst.}$

Table 5
XPS iron content (atomic %) of the carbon-supported iron catalysts.

Sample	Atomic ratio (%)					
	Fe ³⁺	Fe^{2+}	Fe ⁰	Fe ₃ C		
#2 (B-Fe)	39.88	54.84	1.42	3.85		
#3 (C-Fe)	57.11	37.08	1.15	4.66		
#6 (B-Fe-K)	17.11	38.73	31.29	12.87		
#7 (C-Fe-K)	15.76	39.68	31.94	12.62		
#9 (AC-Fe)	15.67	40.22	27.82	16.29		

on the raw biomass and biochar, respectively. Their Fe^0 contents were 31.29 % and 31.94 %, respectively, compared to 1.42 % and 1.15 % for their counterparts prepared without the addition of K_2CO_3 . The addition of K_2CO_3 might cause the reaction of $K_2CO_3 + C \rightarrow K_2O + 2CO$ at a high temperature (i.e., 700 °C) to produce a strong reducing agent of CO that reduced the iron to Fe^{2+} to Fe^0 during calcination. The catalyst (#9) that was produced by impregnating and calcining Fe on the AC had 40.22 % Fe^{2+} , 27.82 % Fe^0 , and 16.29 % Fe_3C , which were much higher than 37.08 % Fe^{2+} , 1.15 % Fe^0 , and 4.66 % Fe_3C for the catalyst produced using the biochar as a support (#3). The strong interaction of iron with highly porous structure of AC at a high temperature could easily reduce and convert iron oxides to zero valent iron (Fe^0) and carbide phase (Fe_3C). The XRD profile (Fig. 1) also confirmed the presence of iron carbide in the catalyst supported on AC.

3.5. Syngas yield and tar removal efficiency of biomass gasification using various catalysts

Figs. 6 and 7 show tar removal efficiency and the yield of syngas during catalytic biomass gasification using the various catalysts. All experiments were carried out at a reaction temperature of 900°C and catalyst to biomass mass ratio of 1:1. Five major tar compounds of benzene, toluene, styrene, phenol, and naphthalene that present in the syngas were quantitatively analyzed. Toluene, phenol, styrene, and naphthalene were usually used to represent the alkylbenzenes, oxygenous aromatics, unsaturated side chain-aromatics, and polycyclic aromatic hydrocarbon in literature, respectively [41]. A series of reactions including Eqs. 2–10 involve in a catalytic gasification process, producing syngas with different compositions using different catalysts and reaction conditions. Our current study did not detect methane in the syngas as the CH₄ as an intermediate was consumed by methane steam reforming reactions (Eqs. 9 and 10).

Hydrogasification reaction
$$C + 2H_2 \rightarrow CH_4$$
 (2)

Boulouard reaction
$$C + CO_2 \rightarrow 2CO$$
 (3)

Water gas reaction
$$C + H_2O \rightarrow CO + H_2$$
 (4)

Water gas reaction
$$CO + H_2O \rightarrow H_2 + CO_2$$
 (5)

Tar cracking reaction
$$Tar \rightarrow C + C_nH_m + gases$$
 (6)

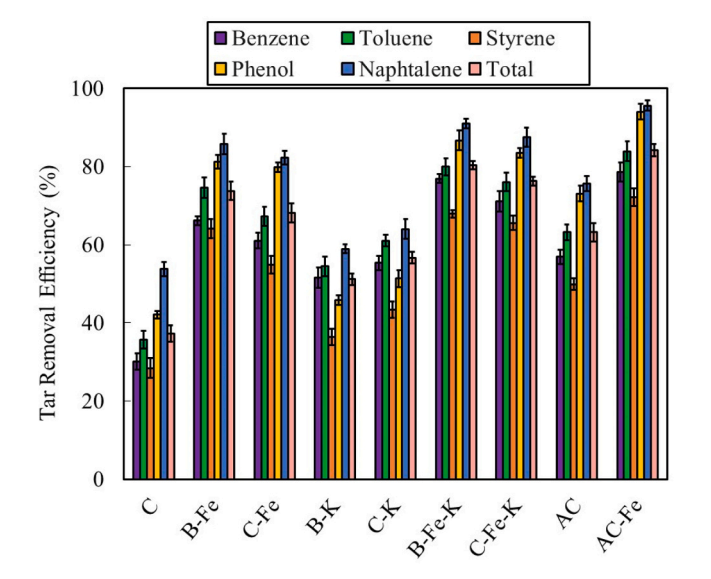


Fig. 6. Tar removal efficiency of the biomass gasification with the various catalysts.

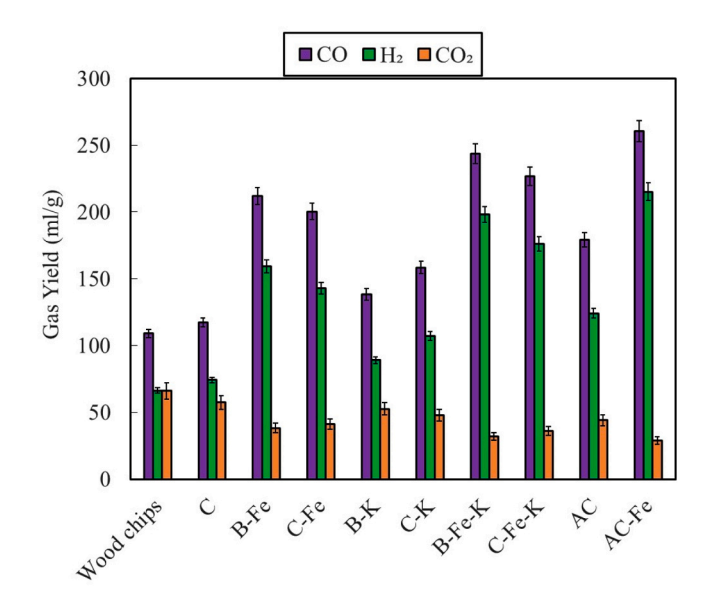


Fig. 7. Syngas yield of the biomass gasification with the various catalysts.

Tar dry reforming reaction
$$C_nH_m+nCO_2 \rightarrow 2nCO + (\frac{m}{2})H_2$$
 (7)

Tar steam reforming reaction
$$C_nH_m+2nH_2O \rightarrow nCO_2 + (2n + \frac{m}{2})H_2$$
 (8)

Methane steam reforming
$$CH_4 + H_2O \rightarrow CO + 3H_2$$
 (9)

Methane steam reforming
$$CH_4 + 2H_2O \rightarrow CO_2 + 4H_2$$
 (10)

The total tar removal efficiency by the AC without iron (#8) was 63.16 %, compared to 37.23 % for the biochar without iron (#2), which means that the AC with the highly porous surface could adsorb more tar compounds for the subsequent cracking than the biochar. Fig. 7 shows that the pyrolysis of the biomass without adding any catalyst produced a total of 241.37 ml/g syngas including 108.98 ml/g CO, 66.41 ml/g H₂, and 65.99 ml/g CO₂. The addition of the biochar could slightly increase the syngas yield to 248.96 ml/g (including 117.36 ml/g CO, 74.22 ml/g H₂, and 57.38 ml/g CO₂). However, the addition of the AC could increase the syngas yield to 347.61 ml/g (containing 179.39 ml/g CO, 124.22 ml/g H₂, and 43.99 ml/g CO₂). The addition of the biochar and AC could decrease CO₂ yield and increase CO and H₂ yields. However, it should be noted that although the highly porous AC can increase the dispersion of iron active sites over the support to enhance the tar removal efficiency and syngas yield, the cost of AC is much higher than biochar.

The biochar and AC impregnated with iron can significantly increase the tar removal efficiency and syngas yield, compared with biochar and AC. Fig. 6 shows that the total tar removal efficiencies were 68.14 % for C-Fe vs 37.23 % for C, and 84.20 % for AC-Fe vs. 63.16 % for AC. Fig. 7 shows that the syngas yield was 384.45 ml/g (200.35 ml/g CO, 142.97 ml/g H₂, and 41.12 ml/g CO₂) for the C-Fe, compared to 248.96 ml/g (117.36 ml/g CO, 74.22 ml/g H₂, and 57.38 ml/g CO₂) for the biochar. The syngas yield for the AC-Fe was 504.62 ml/g (260.42 ml/g CO, 215.27 ml/g H₂ ml/g, and 28.91 ml/g CO₂) which were much higher than the 347.61 ml/g (179.39 ml/g CO and 124.22 ml/g H₂, and 43.99 ml/g CO₂) for the AC. The impregnation of Fe on the biochar and AC could increase the CO and H₂ yields and decrease the CO₂ yield.

The total tar removal efficiency of the gasification catalyzed by the catalyst prepared by impregnating and calcining iron on the raw biomass directly (# 2) was about 73.73 %, which was higher than 68.14 % of the process catalyzed by the catalyst prepared by impregnating and calcining iron on the biochar (#3). This might be attributed to the higher amount of Fe^{2+} on the catalyst #2. As seen from Fig. 7, the yields of CO (212.09 ml/g) and H₂ (159.37 ml/g) produced by the process with the

B-Fe catalyst were higher than those produced by the C-Fe (200.35 ml/g CO and 142.91 ml/g H₂) while there was no significant difference in CO₂ yield (38.25 and 41.12 ml/g). The higher intensity of Fe²⁺ on B-Fe could adsorb more oxygenate compounds and increase the breaking of C–O bands. Iron oxide is a popular oxygen carrier for chemical looping gasification (CLG) of biomass [42]. As the Fe²⁺ is more favorable over Fe³⁺ for catalytic tar removal, the mixture of the reduced state of iron oxide and residual biochar produced in a CLG process could further be used as an effective catalyst for catalytic tar cracking and syngas cleaning.

The co-impregnation of potassium and iron on raw biomass and biochar to form B-Fe-K (#6) and C-Fe-K (#7) could significantly increase the tar removal efficiency and syngas yield. Fig. 6 shows that the total tar removal efficiencies were 80.23 % for B-Fe-K vs 73.73 % for B-Fe, and 76.25 % for C-Fe-K vs. 68.14 % for C-Fe. As shown in Fig. 7, the syngas yield was 473.81 ml/g (243.56 ml/g CO, 198.25 ml/g H₂, and 31.98 ml/g CO_2) for the B-Fe-K, compared to 409.72 ml/g (212.09 ml/g)CO, 159.37 ml/g H_2 , and 38.25 ml/g CO_2) for the B-Fe. Fig. 7 also shows that the syngas for C-Fe-K were 439.03 ml/g (226.83 ml/g CO, 176.20 ml/g H₂, and 35.98 ml/g CO₂) which was much higher than 384.45 ml/g (200.35 ml/g CO, 142.97 ml/g H₂, and 41.12 ml/g CO2) for C-Fe. The improved performance of B-Fe-K and C-Fe-K over B-Fe and C-Fe might be attributed to the increase of Fe²⁺ by the increase of CO as a reducing agent in the presence of K as confirmed by the XPS. Therefore, the high amount of Fe²⁺ promoted by K in B-Fe-K and C-Fe-K that has more tendency to adsorb oxygenate compounds could enhance tar conversion efficiency and syngas yield.

3.6. The effects of catalyst-to-feedstock ratio on tar removal efficiency and syngas yield during catalytic biomass gasification

Figs. 8 and 9 show the effects of catalyst-to-feedstock ratio on tar decomposition efficiency and syngas yield during the biomass gasification over the AC-Fe catalyst at 900°C. As seen in Fig. 8, the tar decomposition efficiency increased with the increase of catalyst-to-feedstock ratio. The tar removal efficiency was increased from 67.83 % to 89.27 % if the catalyst to feedstock ratio increased from 0.5:1–2:1. Because the increase of the amount of the catalyst resulted in increasing the contact time of gaseous tar molecules and the active catalyst sites, resulting in more tar cracking into syngas. The maximum H_2 and CO yields produced by using AC-Fe at catalyst to feedstock ratio of 2:1 were 293.74 and 320.87 ml/g, respectively, which were much higher than 125.47 ml/g H_2 and 203.27 ml/g CO at the ratio of 0.5:1, and 66.40 ml/g H_2 and

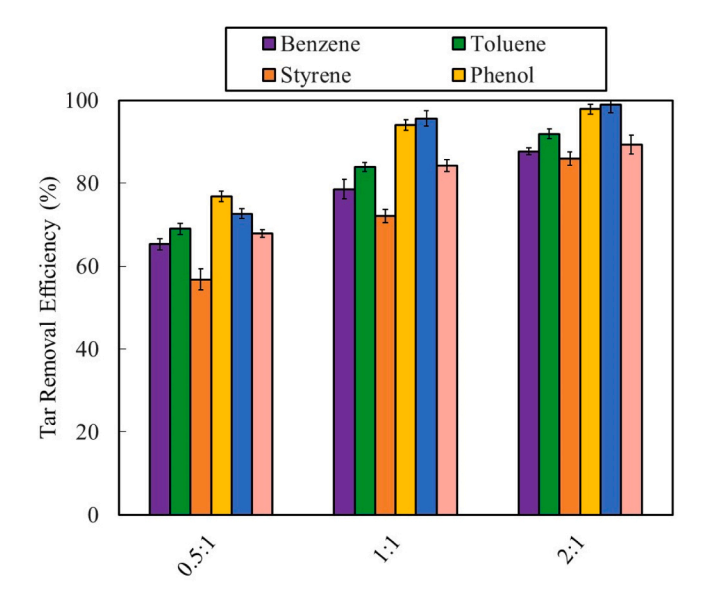


Fig. 8. The effect of catalyst to feedstock ratio on tar removal efficiency.

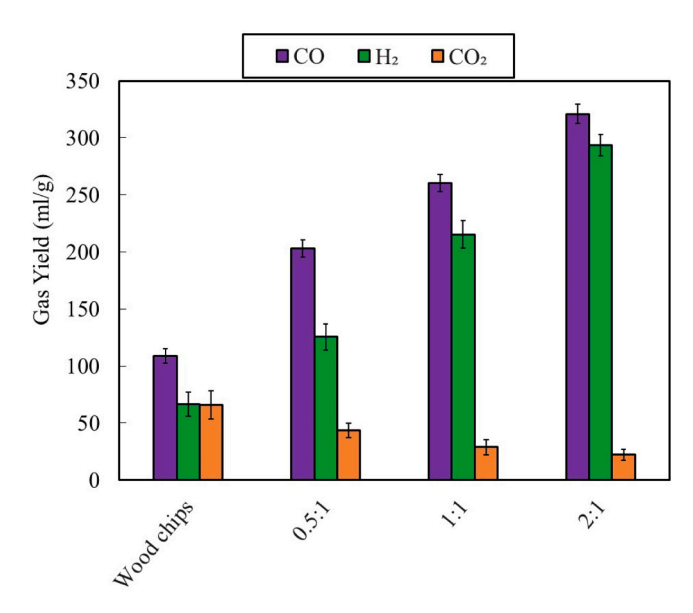


Fig. 9. The effect of catalyst to feedstock ratio on syngas yield.

108.97 ml/g CO for the process without a catalyst.

3.7. The effects of temperature on tar removal efficiency and syngas yield during catalytic biomass gasification

Figs. 10 and 11 show the effects of temperature (800, 900, and 1000°C) on the tar removal efficiency and syngas yield for the process without a catalyst and with an AC-Fe catalyst at a 1:1 catalyst to feed-stock ratio. For the process without a catalyst, the tar removal efficiency increased from 31.12 % to 39.38 % when the temperature increased from 800°C to 1000°C. For the process with the AC-Fe catalyst, the tar removal efficiency increased from 81.14 % to 87.45 % when the temperature increased from 800°C to 1000°C. There was a large variation in the individual tar removal efficiency when the temperature increased. The increasing temperature could increase the cyclic polymerization of some tar components, resulting in the increase of those tar components. It can be seen in Fig. 10(b), the removal efficiencies of naphthalene and phenol during the catalytic biomass gasification over the AC-Fe decreased from 97.59 % to 89.74 %, and 96.48–88.36 %, respectively, when the temperature increased from 800°C to 1000°C.

As seen in Fig. 11, the syngas yield increased with the temperature. This could be attributed to the improved endothermic reverse water-gas shift reaction Eq. (5) at a high temperature. The catalyst-to-feedstock ratio had more significant effect on the syngas yield. Without the catalyst, the CO and H $_2$ yields increased from 98.56 to 122.23 ml/g, and 61.76 ml/g to 74.98 ml/g, respectively, when the temperature increased from 800°C to 1000°C. The yields of CO and H $_2$ were increased from 240.98 to 297.87 ml/g, and 198.76 ml/g to 235.87 ml/g for the catalytic biomass gasification when the temperature increased from 800°C to 1000°C.

4. Conclusions

Different carbonaceous precursors of raw biomass, biochar, and activated carbon (AC) used to prepare carbon supported iron catalysts for catalytic biomass gasification significantly affect the tar removal efficiency and syngas yield. The use of raw biomass and K_2CO_3 during the catalyst preparation could produce more reducing agents such as CO that could reduce the iron to Fe^{2+} and Fe^0 during the calcination. The catalyst prepared by co-impregnating and calcining Fe and K on the raw biomass (B-Fe-K) could remove 80.23 % tar at 900 °C and a catalyst-to-biomass mass ratio of 1:1, which was much higher than 73.73 % for the

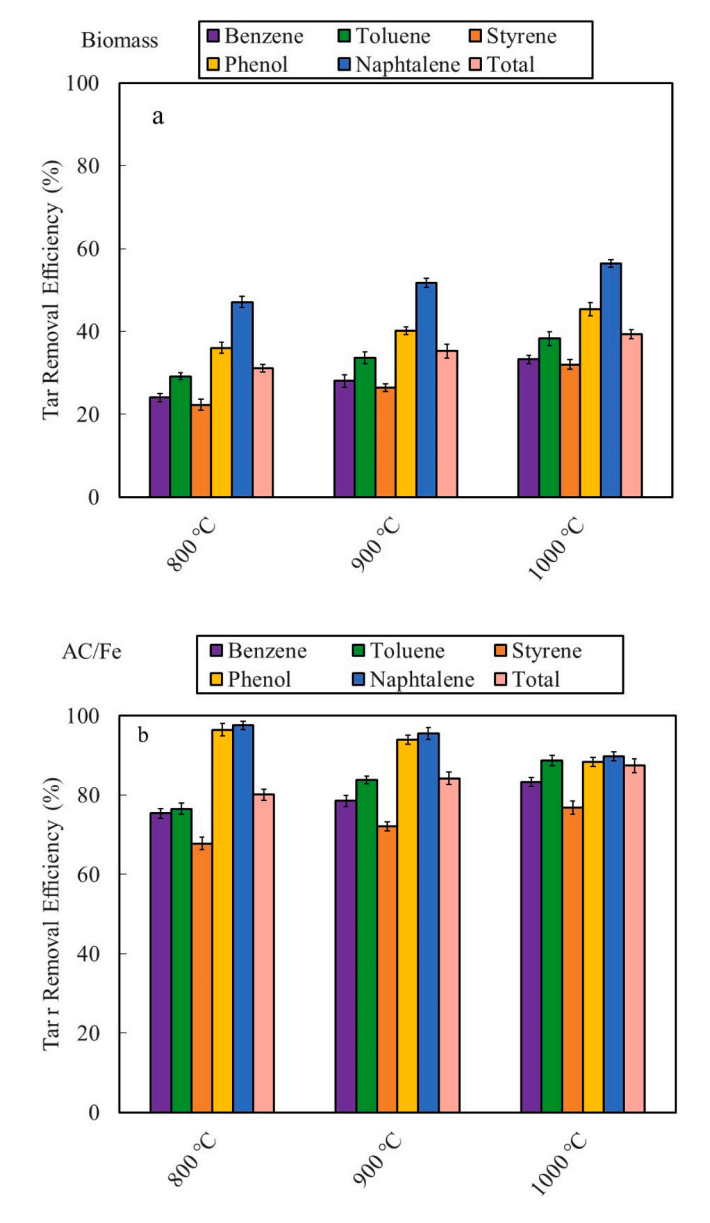
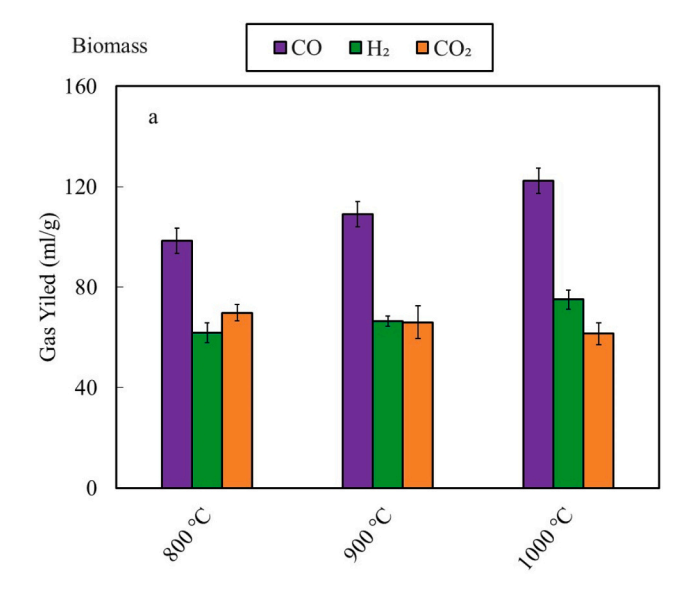


Fig. 10. Effects of reaction temperature on tar removal efficiency with a) no catalyst and b) catalyst to biomass ratio of 1:1.

catalyst of B-Fe without the K promoter, and 76.25 % for the catalyst by co-impregnating and calcining Fe and K on the biochar (C-Fe-K). The iron catalyst supported on the AC achieved the highest total tar removal efficiency of 84.20 %. The highly porous structure of AC could achieve better dispersion and stronger interactions between iron and the support, which could easily reduce iron oxides and produce iron carbide (Fe₃C) at a high temperature to catalyze the tar decomposition. The supports of AC and biochar themselves could also achieve the total tar removal efficiencies of 63.16 % and 37.23 %, respectively. Without any catalyst, the pyrolysis of the biomass only generated 241.37 ml/g syngas (including 108.98 ml/g CO, 66.41 ml/g H_2 , and 65.99 ml/g CO_2). The addition of biochar during the pyrolysis slightly increased the syngas yield to 248.96 ml/g (117.36 ml/g CO, 74.22 ml/g H_2 , and 57.38 ml/g CO₂) while the use of AC could significantly increase the syngas yield to $347.60 \text{ ml/g} (179.39 \text{ ml/g CO}, 124.22 \text{ ml/g H}_2, \text{ and } 43.99 \text{ ml/g CO}_2)$. It was also found that the tar removal efficiency and syngas yield increased with the increase of the catalyst-to-feedstock ratio and gasification temperature. As the Fe²⁺ is more favorable over Fe³⁺ for catalytic tar removal, we will further study the use of the mixture of the reduced iron



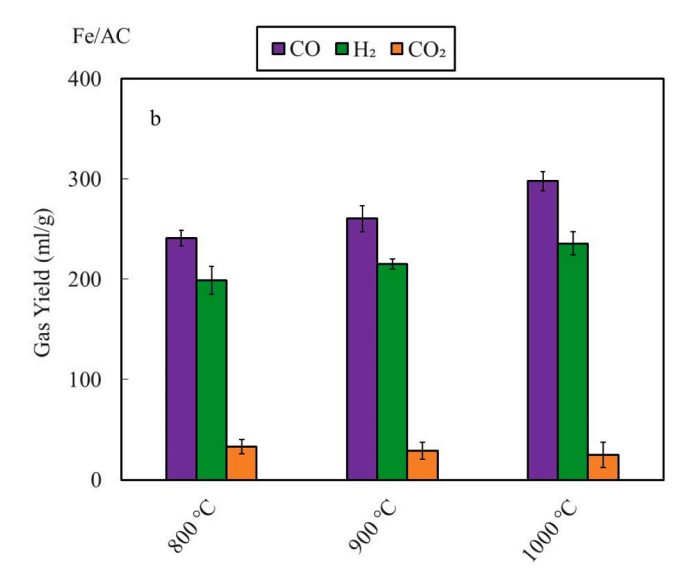


Fig. 11. Effects of reaction temperature on gas yield with a) no catalyst b) catalyst to biomass ratio of 1:1.

oxide and residual biochar from the CLG of biomass for catalytic tar removal and syngas cleaning.

CRediT authorship contribution statement

Conceptualization: Afsaneh Khajeh and Lijun Wang; Methodology, Investigation: Afsaneh Khajeh and Shima Masoumi; Resources: Lijun Wang and Abolghasem Shahbazi; data analysis and Writing – original draft: Afsaneh Khajeh; Writing – review & editing, and Supervision: Lijun Wang; Project administration: Lijun Wang and Abolghasem Shahbazi; Funding acquisition: Lijun Wang and Abolghasem Shahbazi. All authors have read and agreed to the published version of the manuscript.

Declaration of Competing Interest

None.

Data availability

Data will be made available on request.

Acknowledgement

A contribution of North Carolina Agricultural and Technical State University, supported by funds provided by U.S National Scientific Foundation (Grant #: HRD-1736173). Mention of a trade name, proprietary products, or company name is for presentation clarity and does not imply endorsement by the authors or the university.

References

- [1] L.J. Wang, Sustainable Bioenergy Production, CRC Press, Taylor & Francis, Boca Raton, Florida, 2014.
- [2] M. Rafati, L.J. Wang, D.C. Dayton, K. Schimmel, V. Kabadi, A. Shahbazi, Technoeconomic analysis of production of Fisher-Tropsch liquids via biomass gasification: the effects of Fischer-Tropsch catalysts and natural gas co-feeding, Energy Convers. Manag. 133 (2017) 153–166, https://doi.org/10.1016/j.enconman.2016.11.051.
- [3] C. Tsekos, M. del Grosso, W. de Jong, Gasification of woody biomass in a novel indirectly heated bubbling fluidized bed steam reformer, Fuel Process. Technol. 224 (2021), 107003, https://doi.org/10.1016/j.fuproc.2021.107003.
- [4] A.A. Ahmad, N.A. Zawawi, F.H. Kasim, A. Inayat, A., A. Khasri, Assessing the gasification performance of biomass: a review on biomass gasification process conditions, optimization and economic evaluation, Renew. Sustain. Energy Rev. 53 (2016) 1333–1347, https://doi.org/10.1016/j.rser.2015.09.030.
- [5] G. Ravenni, Z. Sarossy, S. Sanna, J. Ahrenfeldt, U.B. Henriksen, Residual gasification char applied to tar reforming in a pilot-scale gasificer: Performance and evolution of char properties for perspective cascade uses, Fuel Process. Technol. 210 (2020), 106546, https://doi.org/10.1016/j.fuproc.2020.106546.
- [6] L. Zhang, Z. Yao, L. Zhao, Z. Li, W. Yi, K. Kang, J. Jia, Synthesis and characterization of different activated biochar catalysts for removal of biomass pyrolysis tar, Energy 232 (2021), 120927, https://doi.org/10.1016/j. energy.2021.120927.
- [7] D. Yao, Q. Hu, D. Wang, H. Yang, C. Wu, X. Wang, H. Chen, Hydrogen production from biomass gasification using biochar as a catalyst/support, Bioresour. Technol. 216 (2016) 159–164, https://doi.org/10.1016/j.biortech.2016.05.011.
- [8] R. Zou, M. Qian, C. Wang, W. Mateo, Y. Wang, L. Dai, X. Lin, Y. Zhao, E. Hao, L. Wang, X. Zhang, X. Kong, R. Ruan, H. Lei, Biochar: from by-products of agroindustrial lignocellulosic waste to tailored carbon-based catalysts for biomass thermochemical conversions, Chem. Eng. J. 441 (2022), 135972, https://doi.org/ 10.1016/j.cei.2022.135972.
- [9] J. Ren, J. Cao, X. Zhao, Y. Liu, Fundamental and applications of char in biomass tar reforming, Fuel Process. Technol. 216 (2021), 106782, https://doi.org/10.1016/j. funcor 2021 106782
- [10] J. Li, Z. Liu, Y. Tian, Y. Zhu, S. Qin, Y. Qiao, Catalytic conversion of gaseous tars using land, coastal and marine biomass-derived char catalysts in a bench-scale downstream combined fixed bed system, Bioresour. Technol. 304 (2020), 122735, https://doi.org/10.1016/j.biortech.2020.122735.
- [11] X. Gao, Z. Wang, J. Ashok, S. Kawi, A comprehensive review of anti-coking, anti-poisoning and anti-sintering catalysts for biomass tar reforming reaction, Chem. Eng. Sci. 7 (2020), 100065, https://doi.org/10.1016/j.cesx.2020.100065.
- [12] A. Rollinson, M. Karmakar, On the reactivity of various biomass species with CO₂ using a standardised methodology for fixed-bed gasification, Chem. Eng. Sci. 128 (2015) 82–91, https://doi.org/10.1016/j.ces.2015.02.007.
- [13] F. Guo, X. Li, Y. Liu, K. Peng, C. Guo, Z. Rao, Catalytic cracking of biomass pyrolysis tar over char-supported catalysts, Energy Convers. Manag. 167 (2018) 81–90, https://doi.org/10.1016/j.enconman.2018.04.094.
- [14] S. Mani, J.R. Kastner, A. Juneja, Catalytic decomposition of toluene using a biomass derived catalyst, Fuel Process. Technol. 114 (2013) 118–125, https://doi. org/10.1016/j.fuproc.2013.03.015.
- [15] Q. Hu, H. Yang, Z. Wu, C.J. Lim, X.T. Bi, H. Chen, Experimental and modeling study of potassium catalyzed gasification of woody char pellet with CO₂, Energy 171 (2019) 678–688, https://doi.org/10.1016/j.energy.2019.01.050.
- [16] S. Wang, Z. Li, X. Bai, W. Yi, P. Fu, Influence of inherent hierarchical porous char with alkali and alkaline earth metallic species on lignin pyrolysis, Bioresour. Technol. 268 (2018) 323–331, https://doi.org/10.1016/j.biortech.2018.07.117.
- [17] B. Tian, S. Du, F. Guo, Y. Dong, S. Mao, L. Qian, Q. Liu, Synthesis of biomimetic monolithic biochar-based catalysts for catalytic decomposition of biomass pyrolysis tar, Energy 222 (2021), 120002, https://doi.org/10.1016/j. energy.2021.120002.
- [18] Y. Shen, J. Wang, X. Ge, M. Chen, By-products recycling for syngas cleanup in biomass pyrolysis—an overview, Renew. Sustain. Energy Rev. 59 (2016) 1246–1268, https://doi.org/10.1016/j.rser.2016.01.077.
- [19] J. Wang, S. Zhang, Y. Su, S. Zhu, Construction of Fe embedded graphene nanoshell/carbon nanofibers catalyst for catalytic cracking of biomass tar: effect of CO₂ etching, Fuel 305 (2021), 121552, https://doi.org/10.1016/j. fuel.2021.121552.

- [20] Y. Shen, Y. Fu, Advances in in situ and ex situ tar reforming with biochar catalysts for clean energy production, Sustain. Energy Fuels 2 (2018) 326–344, https://doi. org/10.1039/C7SE00553A.
- [21] Y. Shen, P. Zhao, Q. Shao, D. Ma, F. Takahashi, K. Yoshikawa, In-situ catalytic conversion of tar using rice husk char-supported nickel-iron catalysts for biomass pyrolysis/gasification, in: Appl. Catal. B, 152, 2014, pp. 140–151, https://doiorg. ncat.idm.oclc.org/10.1016/j.apcatb.2014.01.032.
- [22] Y. Shen, P. Zhao, Q. Shao, F. Takahashi, K. Yoshikawa, In situ catalytic conversion of tar using rice husk char/ash supported nickel-iron catalysts for biomass pyrolytic gasification combined with the mixing-simulation in fluidized-bed gasifier, Appl. Energy 160 (2015) 808–819, https://doi.org/10.1016/j. appergy 2014 10 074
- [23] Y. Shen, M. Chen, T. Sun, J. Jia, Catalytic reforming of pyrolysis tar over metallic nickel nanoparticles embedded in pyrochar, Fuel 159 (2015) 570–579, https://doi. org/10.1016/j.fuel.2015.07.007.
- [24] S. Shukla, R. Chava, S. Appari, A. Bahurudeen, B. Kuncharam, Sustainable use of rice husk for the cleaner production of value-added products, J. Environ. Chem. Eng. 10 (2022), 106899, https://doi.org/10.1016/j.jece.2021.106899.
- [25] L. Gao, Z. Li, W. Yi, Y. Li, P. Zhang, A. Zhang, L. Wang, Impacts of pyrolysis temperature on lead adsorption by cotton stalk-derived biochar and related mechanisms, J. Environ. Chem. Eng. 9 (2021) 2213–3437, https://doi.org/10.1016/j.jece.2021.105602.
- [26] M. Li, Y.S. Zhang, S. Cheng, B. Qu, A. Li, F. Meng, G. Ji, The impact of heating rate on the decomposition kinetics and product distribution of algal waste pyrolysis with in-situ weight measurement, Chem. Eng. J. 457 (2023), 141368, https://doi. org/10.1016/j.cej.2023.141368.
- [27] C. Chen, B. Qu, W. Wang, W. Wang, G. Ji, A. Li, Rice husk and rice straw torrefaction: properties and pyrolysis kinetics of raw and torrefied biomass, Environ. Technol. Innov. 24 (2021), 101872, https://doi.org/10.1016/j. eti.2021.101872.
- [28] C. Chen, R. Yang, X. Wang, B. Qu, M. Zhang, G. Ji, A. Li, Effect of in-situ torrefaction and densification on the properties of pellets from rice husk and rice straw, Chemosphere 289 (2022), 133009, https://doi.org/10.1016/j. chemosphere.2021.133009.
- [29] Z. Khalid, M.N. Siddique, A. Nayeem, T.M. Adyel, S.B. Ismail, M.Z. Ibrahim, Biochar application as sustainable precursors for enhanced anaerobic digestion: a systematic review, J. Environ. Chem. Eng. 9 (2021), 105489, https://doi.org/ 10.1016/j.jece.2021.105489.
- [30] Y. Seow, Y. Tan, N.M. Mubarak, J. Kansedo, M. Khalid, M.L. Ibrahim, M. Ghasemi, A review on biochar production from different biomass wastes by recent carbonization technologies and its sustainable applications, J. Environ. Chem. Eng. 10 (2022), 107017, https://doi.org/10.1016/j.jece.2021.107017.
- [31] L. Jin, X. Bai, Y. Li, C. Dong, H. Hu, X. Li, In-situ catalytic upgrading of coal pyrolysis tar on carbon-based catalyst in a fixed-bed reactor, Fuel Process. Technol. 147 (2016) 41–46, https://doi.org/10.1016/j.fuproc.2015.12.028.
 [32] S. Masoumi, A.K. Dalai, Optimized production and characterization of highly
- [32] S. Masoumi, A.K. Dalai, Optimized production and characterization of highly porous activated carbon from algal-derived hydrochar, J. Clean. Prod. 263 (2020), 121427, https://doi.org/10.1016/j.jclepro.2020.121427.
- [33] G.E. Harimisa, N.W.C. Jusoh, L.S. Tan, K. Shameli, N.A. Ghafar, A. Masudi, Synthesis of potassium hydroxide-treated activated carbon via one-step activation method, in: Proceedings of the Ninth Conference on Emerging Energy & Process Technology 2021, 2259 (2022) 012009, doi:\(\frac{10.1088/1742-6596/2259/1/01 2009\).
- [34] J. Pena, A. Villot, C. Gerente, Pyrolysis chars and physically activated carbons prepared from buckwheat husks for catalytic purification of syngas, Biomass Bioenergy 132 (2020), 105435, https://doi.org/10.1016/j.biombioe.2019.105435.
- [35] S. Hu, L. Jiang, Y. Wang, S. Su, L. Sun, B. Xu, L. He, J. Xiang, Effects of inherent alkali and alkaline earth metallic species on biomass pyrolysis at different temperatures, Bioresour. Technol. 192 (2015) 23–30, https://doi.org/10.1016/j. biortech 2015 05 042
- [36] Y. Shen, Chars as carbonaceous adsorbents/catalysts for tar elimination during biomass pyrolysis or gasification, Renew. Sustain. Energy Rev. 43 (2015) 281–295, https://doi.org/10.1016/j.rser.2014.11.061.
- [37] D.Q. Fu, X.H. Li, W.Y. Li, J. Feng, Catalytic upgrading of coal pyrolysis products over bio-char, Fuel Process. Technol. 176 (2018) 240–248, https://doi.org/ 10.1016/j.fuproc.2018.04.001.
- [38] B.R. Patra, S. Nanda, A.K. Dalai, V. Meda, Slow pyrolysis of agro-food wastes and physicochemical characterization of biofuel products, Chemosphere 285 (2021), 131431, https://doi.org/10.1016/j.chemosphere.2021.131431.
- [39] E. Yagmur, Y. Gokce, S. Tekin, N.I. Semerci, Z. Aktas, Characteristics and comparison of activated carbons prepared from oleaster (Elaeagnus angustifolia L.) fruit using KOH and ZnCl₂, Fuel 267 (2020), 117232, https://doi.org/10.1016/j. fuel.2020.117232.
- [40] K.S. Singh, Reporting physisorption data for gas/solid systems with special reference to the determination of surface area and porosity (Recommendations 1984), Pure Appl. Chem. 57 (1985) 603–619.
- [41] S. Zhao, Y. Luo, Y. Zhang, Y. Long, Experimental investigation of the synergy effect of partial oxidation and bio-char on biomass tar reduction, J. Anal. Appl. Pyrolysis 112 (2015) 262–269, https://doi.org/10.1016/j.jaap.2015.01.016.
- [42] X. Li, L.J. Wang, B. Zhang, A. Khajeh, A. Shahbazi, Iron oxide supported on silicalite-1 as multifunctional oxygen carrier for upgraded biomass chemical looping gasification, Chem. Eng. J. 401 (2020), 125943, https://doi.org/10.1016/ j.cej.2020.125943.